










RESEARCH ARTICLE | JUNE 25 2024

Unveiling a common phase transition pathway of high-density amorphous ices through time-resolved x-ray scattering


Special Collection: [Water: Molecular Origins of its Anomalies](#)


Cheolhee Yang ; Marjorie Ladd-Parada ; Kyeongmin Nam ; Sangmin Jeong; Seonju You ; Tobias Eklund; Alexander Späh; Harshad Pathak ; Jae Hyuk Lee ; Intae Eom; Minseok Kim ; Fivos Perakis ; Anders Nilsson ; Kyung Hwan Kim ; Katrin Amann-Winkel 





J. Chem. Phys. 160, 244503 (2024)
<https://doi.org/10.1063/5.0216904>




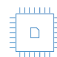
 Nanotechnology & Materials Science


 Optics & Photonics

 Impedance Analysis

 Scanning Probe Microscopy

 Sensors


 Failure Analysis & Semiconductors



Unlock the Full Spectrum. From DC to 8.5 GHz.

Your Application. Measured.

[Find out more](#)



Unveiling a common phase transition pathway of high-density amorphous ices through time-resolved x-ray scattering

Cite as: J. Chem. Phys. 160, 244503 (2024); doi: 10.1063/5.0216904

Submitted: 2 May 2024 • Accepted: 7 June 2024 •

Published Online: 25 June 2024



View Online



Export Citation



CrossMark

Cheolhee Yang,¹ Marjorie Ladd-Parada,² Kyeongmin Nam,¹ Sangmin Jeong,¹ Seonju You,¹ Tobias Eklund,^{3,4,5} Alexander Späh,³ Harshad Pathak,³ Jae Hyuk Lee,⁶ Intae Eom,⁶ Minseok Kim,⁶ Fivos Perakis,³ Anders Nilsson,³ Kyung Hwan Kim,^{1,a)} and Katrin Amann-Winkel^{3,4,5,a)}

AFFILIATIONS

¹ Department of Chemistry, Pohang University of Science and Technology (POSTECH), Pohang, Gyeongbuk 37673, Republic of Korea

² Chemistry Department, Glycoscience Division, Kungliga Tekniska Högskola, Roslagstullsbacken 21, 11421 Stockholm, Sweden

³ Department of Physics, AlbaNova University Center, Stockholm University, SE-10691 Stockholm, Sweden

⁴ Max-Planck-Institute for Polymer Research, 55128 Mainz, Germany

⁵ Institute for Physics, Johannes Gutenberg University Mainz, 55128 Mainz, Germany

⁶ Pohang Accelerator Laboratory, POSTECH, Pohang, Gyeongbuk 37673, Republic of Korea

Note: This paper is part of the JCP Special Topic on Water: Molecular Origins of its Anomalies.

a) Authors to whom correspondence should be addressed: amannk@mpip-mainz.mpg.de and kimkyunghwan@postech.ac.kr

ABSTRACT

Here, we investigate the hypothesis that despite the existence of at least two high-density amorphous ices, only one high-density liquid state exists in water. We prepared a very-high-density amorphous ice (VHDA) sample and rapidly increased its temperature to around 205 ± 10 K using laser-induced isochoric heating. This temperature falls within the so-called “no-man’s land” well above the glass-liquid transition, wherein the IR laser pulse creates a metastable liquid state. Subsequently, this high-density liquid (HDL) state of water decompresses over time, and we examined the time-dependent structural changes using short x-ray pulses from a free electron laser. We observed a liquid–liquid transition to low-density liquid water (LDL) over time scales ranging from 20 ns to 3 μ s, consistent with previous experimental results using expanded high-density amorphous ice (eHDA) as the initial state. In addition, the resulting LDL derived both from VHDA and eHDA displays similar density and degree of inhomogeneity. Our observation supports the idea that regardless of the initial annealing states of the high-density amorphous ices, the same HDL and final LDL states are reached at temperatures around 205 K.

© 2024 Author(s). All article content, except where otherwise noted, is licensed under a Creative Commons Attribution (CC BY) license (<https://creativecommons.org/licenses/by/4.0/>). <https://doi.org/10.1063/5.0216904>

INTRODUCTION

The anomalous behavior of water is discussed in relation to the existence of two liquid states at supercooled temperatures, namely, high- and low-density liquid water (HDL and LDL). Wilhelm Conrad Röntgen speculated about two different configurations in water.¹ This idea was later supported by the experimental finding of two distinct amorphous ices—low-density amorphous (LDA) and high-density amorphous (HDA)—which can be converted into

each other through a first-order-like transition.² The connection between these amorphous solids, their potential liquid counterparts, and their hypothesized relation to the thermodynamic properties of liquid bulk water are still heavily debated.^{3–5} Throughout the years, new experimental findings have added complexity to the debate, particularly with the discovery of a third form of amorphous ice: very-high-density amorphous ice (VHDA).^{6–8} All high-density states share a common origin, initially formed through pressure-induced amorphization, followed by different preparation protocols

within the pressure–temperature phase diagram. Various sub-states can be distinguished by slight differences in structure, density, and thermal stability.^{7,9} However, the exact connection between these states within the potential energy landscape remains unclear.

Previous studies using molecular dynamics (MD) simulations have proposed a theoretical framework wherein the anomalous properties of water at ambient conditions are linked to the existence of a buried critical point at supercooled temperatures and elevated pressure.¹⁰ Below this critical point, HDL and LDL undergo a liquid–liquid phase transition. For many decades, this scenario was only visible using the ST2 water model, a five-site model in which tetrahedrality is built into its constitutive geometry.¹⁰ Recently, this liquid–liquid scenario has also been observed using different computational methods, including more realistic force fields.^{11–16} However, the role played by VHDA remains unclear.¹⁷ Suggestions about multiple liquid–liquid transitions could not be confirmed.¹⁸ Computational studies suggest that VHDA may be the quenched counterpart of HDL¹⁹ and find a continuous transition between the states at very high and low pressures.^{17,20}

Experimental investigations of VHDA and HDA at ambient pressure show that the two forms have a density difference of 9%^{6,7} at 77 K and a clearly different pair correlation function.^{21,22} Neutron and x-ray diffraction data reveal a longer O–O distance, in agreement with Raman measurement, indicating also weaker hydrogen bonds in VHDA compared to HDA at 1 bar.⁶ These measurements show a continuous transition between VHDA and HDA, observed also via decompression at 140 K²³ suggesting that VHDA represents the limiting structure at the high-pressure end. In terms of thermal stability, one also needs to distinguish between unannealed HDA (uHDA) and expanded or equilibrated HDA (eHDA), formed at lower pressure and elevated temperature.^{9,24}

When crystalline ice is pressurized at 77 K, the initial amorphous state is called uHDA. This metastable state does not show any glass transition signature upon warming and transforms into LDA at low temperatures. Although uHDA is structurally very similar to eHDA, the latter can be heated almost 20 K higher before transformation with a preceding increase in heat capacity as a footprint

for a glass transition around 110 K.²⁵ In terms of thermal stability at ambient pressure, VHDA is located between the other states but closely resembles the most relaxed amorphous ice at high pressure. A glass–liquid transition when warming VHDA at elevated pressures was observed around 140 K.²⁶ However, a surprising anomaly between 0.7 and 1.1 GPa was observed by Handle and Loerting.²⁷ While the glass transition in HDA is proposed to increase rather linearly, a sudden drop was observed in the pressure range between 0.7 and 1.1 GPa, where T_g is located at lower temperatures, which was attributed to faster hydrogen bond dynamics.²⁷ Would this imply a rather discontinuous transition between VHDA and HDA? As suggested by Handle and Loerting,²⁸ this scenario then would be related to the existence of a binodal separating VHDA and HDA, located around a pressure of 0.8 GPa. The hypothesis involves a low-temperature critical point above which the distinction between HDA and VHDA disappears.²⁸

The relationship between HDA, VHDA, and their corresponding liquid is still ambiguous, as depicted in the diagram in Fig. 1(a). Our goal is to investigate the ultrafast decompression pathways of VHDA at temperatures far above 160 K. We investigate the timescale of a potential liquid–liquid transition with respect to crystallization. Recent research has reported on the liquid–liquid transition from eHDA, investigated using time-resolved x-ray solution scattering (TRXSS).²⁹ Those experiments successfully accessed short-lived metastable HDL states using ultrafast heating with an IR laser pulse. The wavelength and energy were chosen to increase the temperature in the eHDA sample to around 205 ± 10 K. By varying the time delays between the optical heating pulse (pump) and the x-ray pulse (probe), we probed the structural evolution of the liquid state throughout its subsequent decompression pathway, with the sample free-standing in vacuum. The experimental findings are consistent with computer simulations.^{20,30} Following the same experimental protocol, we now use VHDA as the starting material. The aim of our study is to investigate whether the observed phase transition can be distinguished from the previous experiment while addressing the question of whether HDL water in the phase diagram consists of one or two megabasins.

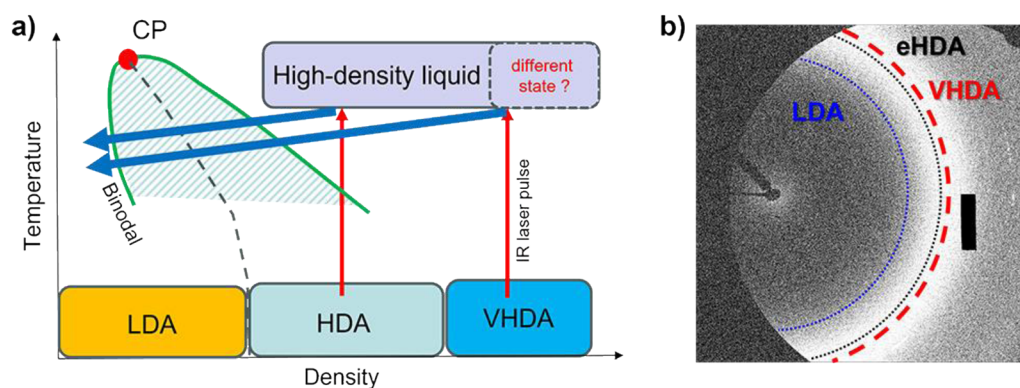


FIG. 1. (a) A schematic illustration of the melting and decompression process followed by isochoric heating of HDA samples. Our interest lies in whether VHDA undergoes the same liquid state as eHDA or not. CP indicates a hypothetical liquid–liquid critical point. (b) WAXS image of VHDA. Approximate peak positions of the diffuse scattering of VHDA (red dashed line), eHDA (black dotted line), and LDA (blue dotted line) are shown as dashed lines as a guide. They exhibit different peak positions reflecting the different densities of the sample.

METHODS

Preparation of amorphous ice samples

VHDA samples were prepared at Stockholm University using a material testing machine (Zwick, Z100 TN) in combination with a 10 mm piston cylinder setup. This setup allows for the implementation of a well-established temperature–pressure protocol, previously utilized in several studies.^{9,22,25,31} Initially, uHDA was generated by pressurizing crystalline ice to 1.6 GPa at 100 K. Subsequently, the uHDA samples were subjected to heating and annealing at 160 K and a pressure of 1.1 GPa, resulting in the formation of VHDA. These VHDA samples were then decompressed to ambient pressure and subsequently stored and transported to PAL-XFEL in South Korea at 78 K (liquid nitrogen temperatures). Under these cryogenic conditions, VHDA remained in a metastable state. To laser-heat the samples, a free-standing ice sample is required. This was achieved by preparing the samples directly inside a small Cu-grid, as previously reported.²⁹ The x-ray scattering peak positions of the VHDA samples and different sample spots measured at 78 K are summarized in Fig. S2 (black square).

Time-resolved x-ray scattering experiment

X-ray scattering experiments employing a pump–probe setup were carried out at the XSS-FXL beamline of PAL-XFEL.^{32,33} VHDA samples on a Cu-grid were placed onto a specially designed sample holder connected to a cryostat (ST-400, Janis Research Company). Temperature control of the cryostat was attained utilizing a silicon diode and a cryogenic temperature controller (DT-670 and Model 335, respectively, Lake Shore Cryotronics). The samples were enclosed within a vacuum chamber maintaining a pressure below 0.1 Pa and cooled with liquid nitrogen, ensuring a base temperature of 115 K. This is necessary in order to obtain a higher final temperature after the T-jump, in comparison to starting from 78 K. Femtosecond optical laser pulses, characterized by a wavelength of 2 μm and energy of 250 μJ /pulse, were generated via an optical parametric amplifier pumped by pulses with a center wavelength of 800 nm from a Ti:sapphire regenerative amplifier. The laser beam was focused to a spot with a diameter of 70 μm (FWHM). Femtosecond x-ray pulses were produced by the x-ray free-electron laser (XFEL) at PAL-XFEL using the self-amplified spontaneous emission (SASE) process. These x-ray pulses had an average energy of 9.7 keV and an energy bandwidth of 0.3% ($\Delta E/E$), focused to a spot measuring 19 \times 32 μm^2 . Spatial overlap between the optical laser pulse and the x-ray pulse occurred at an angle of 20°. X-ray scattering data within the q range of 0.1–3.2 \AA^{-1} were captured utilizing a large area CCD detector (MX225-HS, Rayonix) positioned 250 mm away from the sample. The experimental setup involved inducing ultrafast temperature jumps (T-jumps) within the sample using the optical laser pulse (pump), while the subsequent time-dependent changes were probed using the x-ray pulse (probe). To ensure a sample freshness for each measurement, the sample holder was repositioned before each pump–probe measurement. Prior to the pump–probe measurements, laser-off images (probe-only) were obtained and used as reference scattering patterns for each position. Scattering images were acquired at various time delays ranging from -8.4 ns to 10 μs . The sample volume remains constant during the heating pulse, constrained by the speed of sound, indicating

isochoric heating. Following the isochoric heating, the sample naturally undergoes decompression and cooling, given that the thin ice layer is free-standing in vacuum.

RESULTS AND DISCUSSION

Time-dependent changes of the scattering patterns after ultrafast heating

In agreement with the literature, VHDA samples can be distinguished from eHDA from their different structure, as evidenced by the position of their x-ray scattering halo as shown in Fig. 1(b) (see also Fig. 4(a) for the azimuthally integrated intensity). In Fig. 2, a scattering pattern at each time delay is depicted in each panel as a black solid line. At the shortest time delay (8.4 ns; bottom-left), VHDA undergoes a transition to a liquid state (HDL), based on earlier studies and calibration measurements.²⁹ At a delay of 33.6 ns after the optical laser pulse, the sample begins to undergo a phase transition. This is initially discernible by a slight intensity increase at $q \sim 1.7 \text{\AA}^{-1}$, which corresponds to the characteristic position for the scattering maximum of LDL, indicating the onset of a transition to LDL within tens of nanoseconds. At $\sim 1 \mu\text{s}$, the maximum amount of LDL is observed. Subsequently, LDL undergoes crystallization into ice I within a few microsecond timescales, as evidenced by the time delay of 10 μs . The emergence of HDL, the liquid–liquid transition from HDL to LDL, and the crystallization of LDL mirror our previous eHDA experiments,²⁹ indicating that VHDA undergoes a similar transition pathway as eHDA does. It is noteworthy that we have also confirmed through MD simulations that the resulting state is liquid, with detailed descriptions provided in Ref. 29.

Time-dependent changes of population and SAXS intensity

At various time delays after the T-jump (laser-induced rapid temperature increase), we analyzed wide-angle x-ray scattering

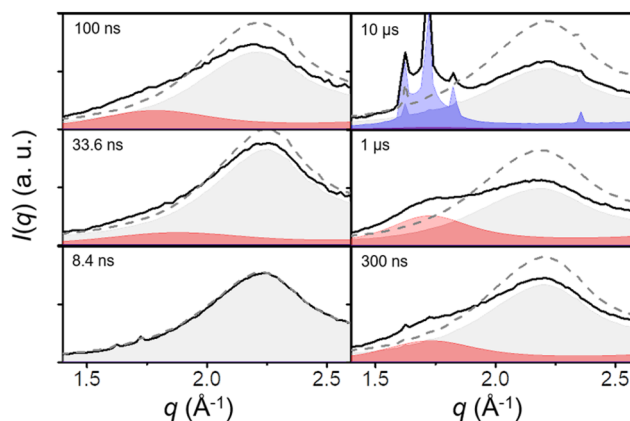


FIG. 2. Scattering patterns of VHDA sample at various time delays after heating. Experimental x-ray scattering intensities, $I(q)$, of VHDA samples measured before (gray dashed line) and after (black solid line) the laser excitation. Data obtained at IR pump/x-ray probe delay times of 8.4 ns–10 μs are shown. The shaded regions in gray, red, and blue correspond to the contributions of HDL, LDL, and crystalline ice, respectively.

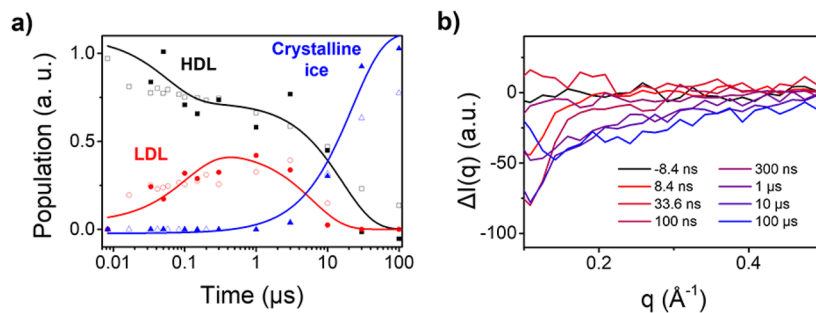


FIG. 3. Time-dependent changes of population and SAXS intensity. (a) Time-dependent population changes of HDL (solid black squares), LDL (solid red circles), and crystalline ice (solid blue triangles) after the isochoric heating of VHDA sample are shown. The solid black, red, and blue lines are shown to guide the eye. The results from eHDA sample are shown together as open symbols for comparison.²⁹ It is notable that both VHDA and eHDA exhibit the same time-dependent changes in population. (b) The difference between the scattering patterns before and after the laser excitation at various time delays from -8.4 ns to 100 μ s.

(WAXS) patterns [Figs. 2 and 3(a)]. The difference scattering curves provide insights into changes induced by laser excitation. The curves revealed contributions from the depletion of HDA (or HDL), the emergence of LDL at early time delays, and the formation of crystalline ice at later time delays. We fitted the difference WAXS curves using a combination of: (1) depletion of HDA, (2) emergence of LDL, and (3) formation of crystalline ice as follows:

$$\Delta I_{\text{model}}(q) = -C_{\text{HDA}}I_{\text{HDA}}(q) + C_{\text{LDL}}I_{\text{LDL}}(q) + C_{\text{crystalline}}I_{\text{crystalline}}(q). \quad (1)$$

For HDA, we utilized the scattering pattern measured prior to the laser pump at the identical position. To represent LDL, we integrate a shifted and broadened LDL component to enhance fitting quality, particularly for early delays. Incorporating the peak shift and broadening of LDL involves introducing q_{shift} and convolving with a Gaussian function defined by c , as follows:

$$\begin{aligned} \Delta I_{\text{model}}(q) = & -C_{\text{HDA}}I_{\text{HDA}}(q) + C_{\text{LDL}} \\ & \times \left\{ \left[A \exp\left(-\frac{q^2}{2c^2}\right) \right] I_{\text{LDL}}(q - q_{\text{shift}}) \right\} \\ & + C_{\text{crystalline}}I_{\text{crystalline}}(q), \end{aligned} \quad (2)$$

where A is a fixed normalization factor. Regarding crystalline ice, we utilized the signal recorded at the same position after 1 ms, which corresponded to the moment when the entire sample had completed its transition to a crystalline ice state. The free parameters for this fitting comprised C_{HDA} , C_{LDL} , q_{shift} , c , and $C_{\text{crystalline}}$. Employing maximum likelihood estimation (MLE) in conjunction with a chi-square (χ^2) estimator, the χ^2 value was calculated using the following equation:

$$\chi^2(C_{\text{HDA}}, C_{\text{LDL}}, C_{\text{crystalline}}) = \frac{1}{N - p - 1} \sum_i \frac{(\Delta I_{\text{model}}(q_i) - \Delta I_{\text{exp}}(q_i))^2}{\sigma_i^2}, \quad (3)$$

where N represents the total number of q points (150), p denotes the number of fitting parameters (3), and σ_i represents the standard deviation of the averaged $I(q)$ at each q_i point. The fitting procedure was conducted using the MINUIT software package,³⁴ with

error values provided by the MINOS algorithm within MINUIT. Following the fitting $I(q)$ for all delays, the values of C_{HDA} , C_{LDL} , and $C_{\text{crystalline}}$ for each time delay were obtained. The temporal changes in C_{HDA} , C_{LDL} , and $C_{\text{crystalline}}$ were subsequently interpreted as indicative of the population changes of HDA, LDL, and crystalline ice over time.

In Fig. 2, the contributions of HDL, LDL, and crystalline ice at each time delay are represented by shaded regions in gray, red, and blue, respectively. The time-dependent changes in the population of HDL, LDL, and crystalline ice are summarized in Fig. 3(a). Results from the eHDA sample are shown together as open symbols for comparison.²⁹ Overall, both states exhibit similar time-dependent changes in population, indicating that VHDA shows qualitatively similar behavior to eHDA after the T-jump. Taking into account the higher density of the initial VHDA state, the sample is expected to take a slightly longer pathway within the P-T-plane during decompression and before reaching the liquid-liquid phase boundary. Comparing VHDA and eHDA at the shortest delay points around 40 ns, the population of the initial state in VHDA changes slower compared to eHDA. This is consistent with a picture of one single HDL free energy megabasin, where the liquid state that is reached after isochoric heating of VHDA relaxes slightly before undergoing a phase transition. Both states (VHDA and eHDA) undergo a phase transition to the same liquid state of LDL before crystallization. In addition, the time scales of emergence and depletion of LDL are similar for both, despite their different starting points in the P-T diagram.

Comparison of WAXS region

The WAXS region shows the first diffraction maximum of the amorphous ice samples. In Fig. 4(a), the current sample is compared with eHDA from our previous study,²⁹ clearly illustrating the characteristic difference between the two amorphous states. The peak positions of the previously reported diffuse scattering peaks of HDA powder samples are 2.14 (eHDA) and 2.28 (VHDA) \AA^{-1} at 77 K.²² Due to the different sample preparation, noticeable discrepancies are observed in the positions of the diffuse scattering peaks. At 78 K, the scattering peak appears around 2.3 \AA^{-1} (Fig. S2, black squares). Our pump-probe experiments, however, started at a base temperature of

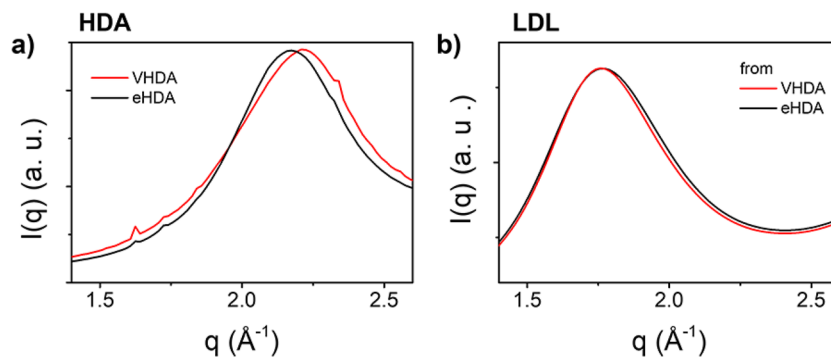


FIG. 4. Comparison in the WAXS region. (a) WAXS patterns of VHDA (red) and eHDA (black) measured before the laser excitation at 115 K. They exhibit different peak positions indicating different densities of the sample. (b) The scattering patterns of LDL are extracted from the fitting analysis explained in the main text. The scattering patterns of LDL generated from the heating of VHDA (red) and eHDA (black) are the same within the experimental error, indicating that a common liquid state is reached regardless of the different starting points.

115 K. While the structure of the eHDA sample is almost not affected by slow heating between 78 and 115 K, VHDA slightly expands in this temperature region. At 115 K, the VHDA peak appears at $\sim 2.21 \text{ \AA}^{-1}$. For our pump-probe studies, we chose this relatively high base temperature to allow for a higher final temperature after the T-jump. The elevated temperature leads to an initial relaxation of the VHDA sample and a shift in the VHDA peak position compared to that at 77 K. This relaxation during slow heating is well known from previous experiments.³⁵ We still consider the sample to belong to the VHDA-family, as the diffraction maximum is distinct from eHDA, and also, our previous experiments demonstrated³⁵ that this sample clearly distinguishes from eHDA in terms of thermal stability, also not showing any sign of a calorimetric glass transition upon slow heating.⁹ We add the temperature as suffix in order to avoid confusion (VHDA₁₁₅).

In contrast to the initial states of eHDA and VHDA₁₁₅, the scattering patterns of LDL generated from the heating of VHDA₁₁₅ and eHDA are identical [Fig. 4(b)], indicating the attainment of

a common liquid state irrespective of the different starting points. The LDL states derived from VHDA₁₁₅ and eHDA₁₁₅ as the starting points are compared, and no significant difference can be detected. This provides additional evidence that VHDA₁₁₅ undergoes similar transitions compared to eHDA₁₁₅.

Comparison of SAXS region

In Fig. 5(a), we show the small-angle x-ray scattering (SAXS) region of VHDA₁₁₅ and eHDA₁₁₅ measured prior to laser excitation at 115 K. The differing SAXS intensities observed suggest variations in sample homogeneity. Specifically, VHDA₁₁₅ exhibits a higher SAXS intensity, implying that it is less homogeneous than eHDA. The larger inhomogeneity might be related to VHDA₁₁₅ being already slightly expanded at 115 K as seen by the shift in the WAXS pattern toward a peak position of 2.21 \AA^{-1} . Additional SAXS measurements on eHDA₇₈ and VHDA₇₈ samples prepared following exactly the same protocol, confirmed this observation (Fig. S1

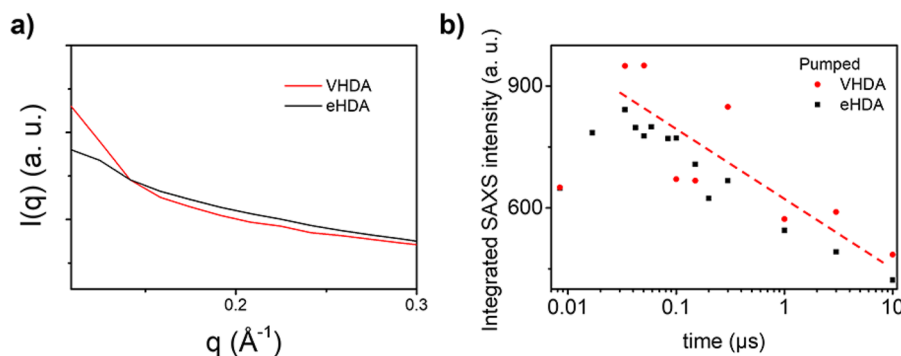


FIG. 5. Comparison in the SAXS region. (a) SAXS patterns of VHDA (red) and eHDA (black) measured at 115 K before the laser excitation are shown together. VHDA₁₁₅ and eHDA₁₁₅ have different SAXS intensities indicating the different inhomogeneity of the samples depending on the initial annealing states. (b) The time-dependent changes in integrated SAXS intensities ranging from $q = 0.1\text{--}0.3 \text{ \AA}^{-1}$ of VHDA₁₁₅ (red) and eHDA₁₁₅ (black) after laser excitation are shown. A red dashed line is provided as a visual guide.

in the [supplementary material](#)). Despite the described difference in the initial state, following the laser excitation, both VHDA₁₁₅ and eHDA₁₁₅ show similar time-dependent changes in integrated SAXS intensities ranging from $q = 0.1\text{--}0.3 \text{ \AA}^{-1}$ [Fig. 5(b)], indicating the attainment of a uniform liquid state.

The difference scattering patterns of VHDA₁₁₅ relative to the initial state are shown in Fig. 3(b). The SAXS intensity begins around zero after the T-jump and progressively decreases to negative values over time. In contrast, the difference value of the SAXS measurements using eHDA as starting material²⁹ shows positive values after the T-jump in the early time delays, followed by a decline to negative values at later time delays. As the SAXS intensity reflects the sample's inhomogeneity, the negative SAXS intensity of the difference scattering pattern indicates the sample's decreased inhomogeneity after the T-jump. The negative SAXS intensity in the early time delays of VHDA₁₁₅, shown in Fig. 5(a), likely stems from its greater initial inhomogeneity compared to eHDA. Following the T-jump, the SAXS profiles of HDAs exhibit comparable intensity levels, suggesting consistent inhomogeneity among the HDAs over time, as they all transition to the same LDL state.

CONCLUSION

The existence of at least two high-density amorphous ices has led to speculations on the potential number of high-density liquids. As a continuation of our earlier pump-probe experiment on eHDA,²⁹ we investigated the ultrafast heating and subsequent decompression of VHDA₁₁₅ at temperatures around 205 K on the timescale from nano- to microseconds. Employing rapid laser-induced isochoric heating of VHDA₁₁₅ to ~ 205 K and monitoring time-dependent structural changes via short x-ray pulses from free electron lasers, we revealed a liquid-liquid transition to LDL within similar time frames as previously observed in eHDA. Although the liquid nature of the post-pump state cannot be directly proven since we use static scattering, MD simulations starting from HDA have clearly demonstrated the attainment of a liquid state.²⁹ The range of the T-jump was validated through experiments on hexagonal ice.²⁹ That is, after the heat jump starting from VHDA₁₁₅, we followed the decompression pathway [as indicated by the blue arrow in Fig. 1(a)]. Just after the optical pump, the structure factor shows the characteristic peak position of a high-density liquid. After around 33 ns, we observed a second shoulder growing at 1.7 \AA^{-1} and an absence of a continuous shift in the high-density peak position. Consistent with our previous argumentation, this behavior suggests the coexistence of two states, provided domains grow to a sufficient size to avoid interference. Similar to the eHDA experiment, we observed a liquid-liquid transition at around $1 \mu\text{s}$ and a clear separate crystallization at similar timescales. It is important to note that the VHDA samples are thicker ($80\text{--}100 \mu\text{m}$) than the eHDA samples previously used, resulting in only a small fraction of VHDA₁₁₅ transforming to LDL (Fig. 2). Even though we have less data points for the statistical analysis of VHDA₁₁₅, in comparison to the eHDA₁₁₅ experiment, the observed trend is unmistakable: a bimodal structure factor develops during decompression, followed by crystallization after $1 \mu\text{s}$.

In addition, the SAXS intensity of both eHDA₁₁₅ and VHDA₁₁₅ exhibits comparable development on an equal timescale. Notably, the initial SAXS intensity of VHDA₁₁₅ at 115 K appears enhanced compared to eHDA₁₁₅ [Fig. 5(a) and Fig. S1], which is likely due to

the partial relaxation at the elevated temperature. Such an enhancement at small scattering angles indicated structural inhomogeneity and is consistent with previous small-angle neutron scattering data.³⁶ We note that, in particular, for the grid samples, this has not been previously observed due to the absence of SAXS measurements on both states over a large enough q -range. Despite differences in density and inhomogeneity evident in the scattering pattern, the resulting LDL from both VHDA₁₁₅ and eHDA₁₁₅ samples proved identical. These findings are consistent with the notion that, regardless of the initial annealing states of high-density amorphous ices, a common liquid state (HDL) is reached after laser heating to around 205 K, subsequently undergoing the same liquid-liquid transition.

SUPPLEMENTARY MATERIAL

The [supplementary material](#) contains additional SAXS data. Figure S1 shows scattering intensities at small q obtained from additional VHDA and eHDA samples at 78 K. Figure S2 shows the peak positions of VHDA diffuse scattering in the pre-pump scattering pattern.

ACKNOWLEDGMENTS

K.A.-W. acknowledged funding by the Ragnar Söderbergs Stiftelse (Grant No. S14/20). This work was also supported by the National Research Foundation of Korea (NRF) grant funded by the Korea Government (MSIT) (Grant Nos. NRF-2020R1A5A1019141 and RS-2024-00348773) (K.H.K., C.Y., K.N., S.J., and S.Y.). The experiments were performed at beamline XSS-FXL of PAL-XFEL (proposals 2018-1st-XSS-009, 2018-2nd-XSS-006, and 2019-1st-XSS-008) funded by the Korea government (MSIT). This work has been supported by a European Research Council Advanced Grant under Project No. 407 667205 (A.N.) and a Swedish National Research Council Grant No. 2013-8823 (A.N.).

AUTHOR DECLARATIONS

Conflict of Interest

The authors have no conflicts to disclose.

Author Contributions

Cheolhee Yang: Data curation (equal); Formal analysis (lead); Investigation (equal); Software (equal); Visualization (equal); Writing – original draft (equal); Writing – review & editing (equal). **Marjorie Ladd-Parada:** Investigation (equal); Methodology (equal); Writing – review & editing (equal). **Kyeongmin Nam:** Data curation (equal); Formal analysis (equal); Software (equal). **Sangmin Jeong:** Data curation (equal); Formal analysis (equal); Software (equal). **Seonju You:** Data curation (equal); Formal analysis (equal); Software (equal). **Tobias Eklund:** Investigation (equal); Methodology (equal). **Alexander Späh:** Conceptualization (equal); Investigation (equal); Methodology (equal). **Harshad Pathak:** Conceptualization (equal); Data curation (equal); Investigation (equal); Methodology (equal); Writing – review & editing (supporting). **Jaе Hyuk Lee:** Investigation (equal); Methodology (equal); Resources (equal).

Intae Eom: Investigation (equal); Methodology (equal); Resources (equal). **Minseok Kim:** Investigation (equal); Methodology (equal); Resources (equal). **Fivos Perakis:** Conceptualization (equal); Investigation (equal); Methodology (equal); Writing – review & editing (equal). **Anders Nilsson:** Conceptualization (equal); Funding acquisition (lead); Investigation (equal); Methodology (equal); Project administration (lead); Supervision (lead); Writing – review & editing (equal). **Kyung Hwan Kim:** Conceptualization (equal); Data curation (equal); Formal analysis (equal); Funding acquisition (equal); Investigation (equal); Methodology (lead); Resources (equal); Software (equal); Supervision (equal); Validation (equal); Writing – original draft (equal); Writing – review & editing (lead). **Katrin Amann-Winkel:** Conceptualization (lead); Data curation (equal); Funding acquisition (equal); Investigation (equal); Methodology (equal); Resources (equal); Supervision (equal); Validation (equal); Visualization (equal); Writing – original draft (equal); Writing – review & editing (equal).

DATA AVAILABILITY

The data that support the findings of this study are openly available in Zenodo <https://doi.org/10.5281/zenodo.11492005>.

REFERENCES

- W. C. Röntgen, “Ueber den Einfluss des Druckes auf die Viscosität der Flüssigkeiten, speciell des Wassers,” *Ann. Phys.* **258**, 510–518 (1884).
- O. Mishima, “Reversible first-order transition between two H₂O amorphs at ~0.2 GPa and ~135 K,” *J. Chem. Phys.* **100**, 5910–5912 (1994).
- P. Gallo, K. Amann-Winkel, C. A. Angell, M. A. Anisimov, F. Caupin, C. Chakravarty, E. Lascaris, T. Loerting, A. Z. Panagiotopoulos, J. Russo, J. A. Sellberg, H. E. Stanley, H. Tanaka, C. Vega, L. M. Xu, and L. G. M. Pettersson, “Water: A tale of two liquids,” *Chem. Rev.* **116**, 7463–7500 (2016).
- P. Gallo, J. Bachler, L. E. Bove, R. Böhmer, G. Camisasca, L. E. Coronas, H. R. Corti, I. de Almeida Ribeiro, M. de Koning, G. Franzese, V. Fuentes-Landete, C. Gainaru, T. Loerting, J. M. M. de Oca, P. H. Poole, M. Rovere, F. Sciortino, C. M. Tonauer, and G. A. Appignanesi, “Advances in the study of supercooled water,” *Eur. Phys. J. E* **44**, 143 (2021).
- F. Caupin, “Predictions for the properties of water below its homogeneous crystallization temperature revisited,” *J. Non-Cryst. Solids: X* **14**, 100090 (2022).
- T. Loerting, C. Salzmann, I. Kohl, E. Mayer, and A. Hallbrucker, “A second distinct structural “state” of high-density amorphous ice at 77 K and 1 bar,” *Phys. Chem. Chem. Phys.* **3**, 5355–5357 (2001).
- T. Loerting, K. Winkel, M. Seidl, M. Bauer, C. Mitterdorfer, P. H. Handle, C. G. Salzmann, E. Mayer, J. L. Finney, and D. T. Bowron, “How many amorphous ices are there?,” *Phys. Chem. Chem. Phys.* **13**, 8783–8794 (2011).
- J. N. Stern and T. Loerting, “On the crystallisation temperature of very high-density amorphous ice,” *Phys. Chem. Chem. Phys.* **20**, 12589–12598 (2018).
- K. Winkel, E. Mayer, and T. Loerting, “Equilibrated high-density amorphous ice and its first-order transition to the low-density form,” *J. Phys. Chem. B* **115**, 14141–14148 (2011).
- P. H. Poole, F. Sciortino, U. Essmann, and H. E. Stanley, “Phase behaviour of metastable water,” *Nature* **360**, 324–328 (1992).
- P. G. Debenedetti, F. Sciortino, and G. H. Zerze, “Second critical point in two realistic models of water,” *Science* **369**, 289–292 (2020).
- F. Sciortino, I. Saika-Voivod, and P. H. Poole, “Study of the ST2 model of water close to the liquid-liquid critical point,” *Phys. Chem. Chem. Phys.* **13**, 19759–19764 (2011).
- T. E. Gartner, L. F. Zhang, P. M. Piaggi, R. Car, A. Z. Panagiotopoulos, and P. G. Debenedetti, “Signatures of a liquid-liquid transition in an ab initio deep neural network model for water,” *Proc. Natl. Acad. Sci. U. S. A.* **117**, 26040–26046 (2020).
- J. Weis, F. Sciortino, A. Z. Panagiotopoulos, and P. G. Debenedetti, “Liquid-liquid criticality in the WAIL water model,” *J. Chem. Phys.* **157**, 024502 (2022).
- T. E. Gartner, P. M. Piaggi, R. Car, A. Z. Panagiotopoulos, and P. G. Debenedetti, “Liquid-liquid transition in water from first principles,” *Phys. Rev. Lett.* **129**, 255702 (2022).
- F. Sciortino, T. Gartner, and P. G. Debenedetti, “Free-energy landscape and spinodals for the liquid-liquid transition of the TIP4P/2005 and TIP4P/Ice models of water,” *J. Chem. Phys.* **160**, 104501 (2024).
- R. Foffi and F. Sciortino, “Structure of high-pressure supercooled and glassy water,” *Phys. Rev. Lett.* **127**, 175502 (2021).
- I. Brovchenko and A. Oleinikova, “Multiple phases of liquid water,” *ChemPhysChem* **9**, 2660–2675 (2008).
- N. Giovambattista, H. E. Stanley, and F. Sciortino, “Relation between the high density phase and the very-high density phase of amorphous solid water,” *Phys. Rev. Lett.* **94**, 107803 (2005).
- N. Giovambattista and P. H. Poole, “Liquid-liquid phase transition in simulations of ultrafast heating and decompression of amorphous ice,” *J. Non-Cryst. Solids: X* **11-12**, 100067 (2021).
- J. L. Finney, D. T. Bowron, A. K. Soper, T. Loerting, E. Mayer, and A. Hallbrucker, “Structure of a new dense amorphous ice,” *Phys. Rev. Lett.* **89**, 205503 (2002).
- D. Mariedahl, F. Perakis, A. Späh, H. Pathak, K. H. Kim, G. Camisasca, D. Schlesinger, C. Benmore, L. G. M. Pettersson, A. Nilsson, and K. Amann-Winkel, “X-Ray scattering and O–O pair-distribution functions of amorphous ices,” *J. Phys. Chem. B* **122**, 7616–7624 (2018).
- K. Winkel, M. S. Elsaesser, E. Mayer, and T. Loerting, “Water polyamorphism: Reversibility and (dis)continuity,” *J. Chem. Phys.* **128**, 044510 (2008).
- R. J. Nelmes, J. S. Loveday, T. Strässle, C. L. Bull, M. Guthrie, G. Hamel, and S. Klotz, “Annealed high-density amorphous ice under pressure,” *Nat. Phys.* **2**, 414–418 (2006).
- K. Amann-Winkel, C. Gainaru, P. H. Handle, M. Seidl, H. Nelson, R. Böhmer, and T. Loerting, “Water’s second glass transition,” *Proc. Natl. Acad. Sci. U. S. A.* **110**, 17720–17725 (2013).
- O. Andersson, “Glass-liquid transition of water at high pressure,” *Proc. Natl. Acad. Sci. U. S. A.* **108**, 11013–11016 (2011).
- P. H. Handle and T. Loerting, “Dynamics anomaly in high-density amorphous ice between 0.7 and 1.1 GPa,” *Phys. Rev. B* **93**, 064204 (2016).
- P. H. Handle and T. Loerting, “Experimental study of the polyamorphism of water. II. The isobaric transitions between HDA and VHDA at intermediate and high pressures,” *J. Chem. Phys.* **148**, 124509 (2018).
- K. H. Kim, K. Amann-Winkel, N. Giovambattista, A. Späh, F. Perakis, H. Pathak, M. L. Parada, C. Yang, D. Mariedahl, T. Eklund, T. J. Lane, S. You, S. Jeong, M. Weston, J. H. Lee, I. Eom, M. Kim, J. Park, S. H. Chun, P. H. Poole, and A. Nilsson, “Experimental observation of the liquid-liquid transition in bulk supercooled water under pressure,” *Science* **370**, 978–982 (2020).
- E. M. Mollica, J. Russo, H. E. Stanley, and F. Sciortino, “Decompression dynamics of high density amorphous ice above and below the liquid-liquid critical point,” *J. Non-Cryst. Solids: X* **13**, 100081 (2022).
- F. Perakis, K. Amann-Winkel, F. Lehmkuhler, M. Sprung, D. Mariedahl, J. A. Sellberg, H. Pathak, A. Späh, F. Cavalca, D. Schlesinger, A. Ricci, A. Jain, B. Massani, F. Aubree, C. J. Benmore, T. Loerting, G. Grübel, L. G. M. Pettersson, and A. Nilsson, “Diffusive dynamics during the high-to-low density transition in amorphous ice,” *Proc. Natl. Acad. Sci. U. S. A.* **114**, 8193–8198 (2017).
- I. S. Ko, H. S. Kang, H. Heo, C. Kim, G. Kim, C. K. Min, H. Yang, S. Y. Baek, H. J. Choi, G. Mun, B. R. Park, Y. J. Suh, D. C. Shin, J. Hu, J. Hong, S. Jung, S. H. Kim, K. Kim, D. Na, S. S. Park, Y. J. Park, Y. G. Jung, S. H. Jeong, H. G. Lee, S. Lee, S. Lee, B. Oh, H. S. Suh, J. H. Han, M. H. Kim, N. S. Jung, Y. C. Kim, M. S. Lee, B. H. Lee, C. W. Sung, I. S. Mok, J. M. Yang, Y. W. Parc, W. W. Lee, C. S. Lee, H. Shin, J. H. Kim, Y. Kim, J. H. Lee, S. Y. Park, J. Kim, J. Park, I. Eom, S. Rah, S. Kim, K. H. Nam, J. Park, J. Park, S. Kim, S. Kwon, R. An, S. H. Park, K. S. Kim, H. Hyun, S. N. Kim, S. Kim, C. J. Yu, B. S. Kim, T. H. Kang, K. W. Kim, S. H. Kim, H. S. Lee, H. S. Lee, K. H. Park, T. Y. Koo, D. E. Kim, and K. B. Lee, “Construction and commissioning of PAL-XFEL facility,” *Appl. Sci.* **7**, 479 (2017).
- H. S. Kang, C. K. Min, H. Heo, C. Kim, H. Yang, G. Kim, I. Nam, S. Y. Baek, H. J. Choi, G. Mun, B. R. Park, Y. J. Suh, D. C. Shin, J. Hu, J. Hong, S. Jung, S. H.

Kim, K. Kim, D. Na, S. S. Park, Y. J. Park, J. H. Han, Y. G. Jung, S. H. Jeong, H. G. Lee, S. Lee, S. Lee, W. W. Lee, B. Oh, H. S. Suh, Y. W. Parc, S. J. Park, M. H. Kim, N. S. Jung, Y. C. Kim, M. S. Lee, B. H. Lee, C. W. Sung, I. S. Mok, J. M. Yang, C. S. Lee, H. Shin, J. H. Kim, Y. Kim, J. H. Lee, S. Y. Park, J. Kim, J. Park, I. Eom, S. Rah, S. Kim, K. H. Nam, J. Park, J. Park, S. Kim, S. Kwon, S. H. Park, K. S. Kim, H. Hyun, S. N. Kim, S. Kim, S. M. Hwang, M. J. Kim, C. Y. Lim, C. J. Yu, B. S. Kim, T. H. Kang, K. W. Kim, S. H. Kim, H. S. Lee, H. S. Lee, K. H. Park, T. Y. Koo, D. E. Kim, and I. S. Ko, "Hard X-ray free-electron laser with femtosecond-scale timing jitter," *Nat. Photonics* **11**, 708–713 (2017).

³⁴F. James and M. Roos, "Minuit - A system for function minimization and analysis of the parameter errors and correlations," *Comput. Phys. Commun.* **10**, 343–367 (1975).

³⁵D. Mariedahl, F. Perakis, A. Späh, H. Pathak, K. H. Kim, C. Benmore, A. Nilsson, and K. Amann-Winkel, "X-ray studies of the transformation from high- to low-density amorphous water," *Philos. Trans. R. Soc., A* **377**, 20180164 (2019).

³⁶M. M. Koza, "Transient pronounced density variation in amorphous ice structures," *Z. Phys. Chem.* **223**, 979–1000 (2009).